P. Martin,[1,] H. Ahmed,[1,2] D. Doria,[1,3] A. Alejo,[1,4] R. Clarke,[2] S. Ferguson,[1] J. Fernández-Tobias,[2,5] R. R. Freeman,[6] J. Fuchs,[7] A. Green,[1] J. S. Green,[2] D. Gwynne,[1] F. Hanton,[1] J. Jarrett,[8] D. Jung,[1] K. F. Kakolee,[1,9] A. G. Krygier,[6] C. L. S. Lewis,[1] A. McIlvenny,[1] P. McKenna,[8] J. T. Morrison,[10] Z. Najmudin,[11] K. Naughton,[1] G. Nersisyan,[1] P. Norreys,[12] M. Notley,[2] M. Roth,[13] J. A. Ruiz,[5] C. Scullion,[1] M. Zepf,[14,15,16] S. Zhai,[1,17] M. Borghesi,[1] and S. Kar[1,]

Centre for Plasma Physics, School of Mathematics and Physics, Queen's University Belfast, Belfast BT7 1NN, United Kingdom

Central Laser Facility, Rutherford Appleton Laboratory, Didcot, Oxfordshire OX11 0QX, United Kingdom

Extreme Light Infrastructure (ELI-NP), and Horia Hulubei National Institute for R&D in Physics and Nuclear Engineering (IFIN-HH), Str. Reatorului No. 30, 077125 Bucharest-Magurele, Romania

IGFAE, Universidade de Santiago de Compostela, 27002 Santiago de Compostela, Spain

Instituto de Fusion Nuclear, Universidad Politécnica de Madrid, 28040 Madrid, Spain

Department of Physics, The Ohio State University, Columbus, Ohio 43210, USA

LULI, École Polytechnique, CNRS, CEA, UPMC, 91128 Palaiseau, France

Department of Physics, SUPA, University of Strathclyde, Glasgow G4 0NG, United Kingdom

Department of Physics, Jagannath University, Dhaka-1100, Bangladesh

Department of Electrical and Computer Engineering, Colorado State University, Fort Collins, CO 80523, USA

Blackett Laboratory, Department of Physics, Imperial College, London SW7 2AZ, United Kingdom

Department of Physics, University of Oxford, Oxford OX1 3PU, United Kingdom

Institut für Kernphysik, Technische Universität Darmstadt, Schloßgartenstrasse 9, 64289 Darmstadt, Germany

Helmholtz Institut Jena, 07743 Jena, Germany

Institute for Quantumoptics, University of Jena, 07743 Jena, Germany

GSI GmbH, 64291 Darmstadt, Germany

Department of Mathematics and Physics, Shanghai Normal University, Shanghai 200234, China

Corresponding author: p.martin@qub.ac.uk
Electronic mail: s.kar@qub.ac.uk

$$\left(\frac{}{}\right) \times \frac{}{} \times \quad L\left(\frac{QL}{2^G-1}-\frac{1}{2}\right)$$

$et\ al.$ $et\ al.$ $et\ al.$ $et\ al.$
$et\ al.$ $et\ al.$

$\sim$

$\sim$

$\left(-\right)^{-}$.

Dep

$\int^{w}$ — $\left(--\right)$

Left axis

et al. *et al.* *et al.*
et al.

et al.
Right axis
Dep

$\sim$

$\pm$

$$\int^{w} \frac{\frac{dE}{dz} \qquad \left(-\frac{z}{L}\right)}{\frac{dE}{dz}}$$

$\sim$

$\sim$

$-$ $\times$

$\sim$

$$\int^{w} - \left(\frac{\left(-\frac{z}{L}\right)}{\frac{dE}{dz}} \qquad \right)$$

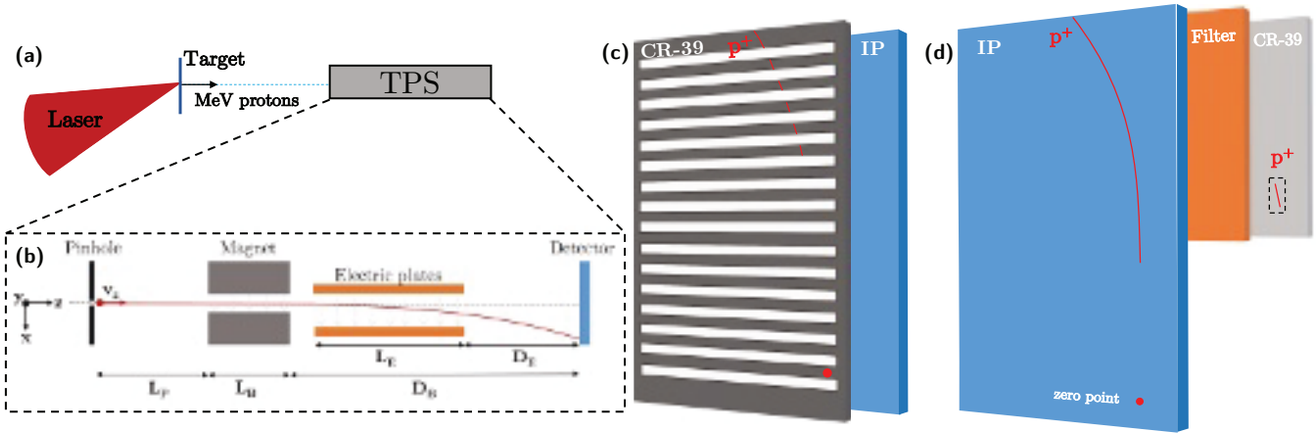

FIG. 3. (a) Schematic of a typical experimental setup used at each laser system. (b) Schematic of a Thomson parabola spectrometer. (c) Slotted CR-39/IP detector assembly used to calibrate low energy (sub-10 MeV) protons in Experiments 1 and 2 listed in Table I. (d) The layout of the IP/filter/CR-39 detector assembly from Experiment 3 for the calibration of protons above 10 MeV.

~10 μm thick Al targets, producing protons at energies of several MeV. For the IP calibration, Thomson parabola spectrometers, coupled with an IP as the primary particle detector were used. A schematic of the experimental setup at these campaigns is shown in Figure 3(a), and a description of the details of each experiment is listed in Table I, with each experiment assigned a number from 1–3 for referencing later. TPS are spectrometers which use magnetic and electric fields to separate charged particles according to their energy, as well as their charge-mass ratio (q/m). The ions form a parabolic trace along the detector plane, with their x and y positions with respect to zero deflection determined by (6) and (7).

$$y = \frac{q}{mv_z} B_0 L_B \left(\frac{L_B}{2} + D_B \right), \tag{6}$$

$$x = \frac{q}{mv_z^2} E_0 L_E \left(\frac{L_E}{2} + D_E \right), \tag{7}$$

where q is the ion charge, m is the mass, v_z is the velocity, B_0 and E_0 are the magnetic and electric field strengths, respectively, and L_B, L_E, D_E, and D_B are the distances as defined in Figure 3(b). Thus, the vertical distance on the detector above the zero point will determine the energy of the ion, the PSL value of which can be easily extracted. In order to determine the number of protons at that point, CR-39 can be used in conjunction with the IP. CR-39 is a solid state detector that, when etched in a sodium hydroxide (NaOH) bath for a certain time, will display the ion damage tracks that are then visible through a microscope[20,42], and can be counted manually or by using image analysis software.

The visibility of the etched pits in the CR-39 depends on the LET of the particle entering it, and due to the nature of the Bragg peak that is characteristic of ion stopping in matter, most of the ions kinetic energy is lost at the end of its trajectory. Thus, ion damage tracks in CR-39 are usually only visible if the ion fully stops inside the material. For the 1 mm thick CR-39 used in this work, protons below ~10 MeV stop inside the detector. Therefore, for protons of energies below 10 MeV, a slotted piece of CR-39 was placed in front of the IP in experiments 1 and 2, as used in Refs.[22,23,27,30,33,43] and shown in Fig. 3(c). In this case, the PSL values immediately adjacent to the edges of the CR-39 slots could be integrated across the proton trace. The proton pits at the CR-39 edge would then be binned into areas of the same size as the sampling interval on the scanned IP (25 μm), and integrated across the slot edge. This enables a direct comparison between PSL and the number of pits counted at the slot edges, to provide a value of the PSL per incident proton at that energy. This technique has been used in the past successfully for the calibration of low energy (<0.2 MeV) protons[27], as well as deuterium[30], carbon[27,33], titanium[34], and gold[44] ions.

For the calibration of higher energy protons, it would not be possible to use CR-39 in front of the IP. Therefore, in Experiment 3 CR-39 were used behind the IP with a suitable thickness of iron or copper filter in between, as shown in Fig. 3(d). The filter reduces the energies of the transmitted protons to below 10 MeV, in order for them to stop in the CR-39 and be visible after etching. The range of energies which could be detected at the front and back surfaces of the CR-39 with a set of filters, as listed in Table II, was determined through SRIM simulations.

The minimum and maximum energies shown in Table II determine the energy range of protons which will show up in CR-39 after etching, resulting in a "streak" of pits that aligns with a small section of the proton trace on the IP. The CR-39 was etched in a NaOH solution at a concentration of 6.5 mol/kg at 85°C for up to 80 minutes, and the pits counted on both the front and back surfaces. An image of the streak of proton pits on a CR-39 is shown in Fig. 5 along with the image of the IP from the same

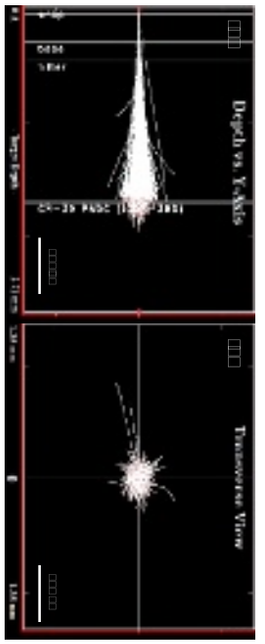

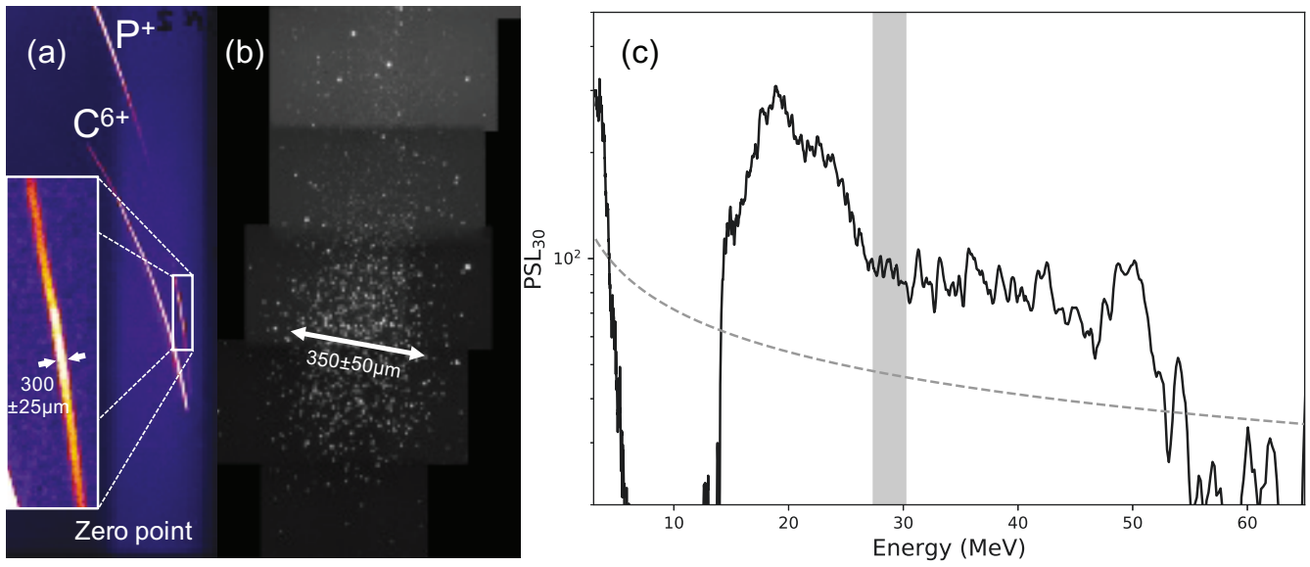

FIG. 5. (a) Scanned IP image converted to PSL, with each trace corresponding to ions with a specific q/m labelled. The inset shows a zoomed in portion of the proton trace, which was measured to be (300 ± 25) μm wide. Behind the IP was a 1250 μm Cu filter and CR-39. (b) Microscope image of the proton pits on the front surface of the CR-39 after etching at $\times$20 magnification. The width of the pit streak was measured to be $\sim(350 \pm 50)$ μm. (c) Background subtracted PSL_{30} profile across the proton trace in the IP shown in (a). The shaded region indicates the energy range which the CR-39 detected protons. The detection limit of the IP is shown as the dashed grey line.

fits reasonably well, but deviates from the observed true response at high energies.

From the model described by Lelasseux *et al.*[38], using their value for $kB = 0.15$ Å/eV, the least squares fitting gave a value of $\alpha = 0.5 \pm 0.01$ PSL/MeV. However, the fitting of this curve did not match well with our lower energy data. In order to improve the accuracy of the model, a least squares fitting was performed while varying both α and kB. This gave a new set of values of the model parameters as $\alpha = 0.44 \pm 0.02$ PSL/MeV, and $kB = 0.04 \pm 0.03$ Å/eV. Our new value of kB is significantly smaller than that originally proposed by Lelasseux, and has a large relative error, which suggests that the contribution of phosphor quenching to the IP response can be lower than originally anticipated. The curves generated by these new values are shown in Fig. 6(b), showing a good agreement between the models and our experimental data.

Using these models require running Monte Carlo simulations to determine proton energy deposition in the active layer. In lieu of this, one may prefer using a best fit function to the data shown in Fig. 6(b), which gives two power laws with different energy limits:

$$PSL_{30}/p^{+} = \begin{cases} 0.151\ E_p^{0.6} & (\mathrm{E_p} < 1.6\ \mathrm{MeV}) \\ 0.284\ E_p^{-0.75} & (\mathrm{E_p} \geq 1.6\ \mathrm{MeV}) \end{cases}, \quad (8)$$

where E_p is the proton energy given in MeV. As there are no experimental data for energies below 1.6 MeV (corresponding to the peak in energy deposition in the active layer — see Fig. 2), the response equation was determined by fitting to the data reported by other works (down to 0.5 MeV), shown in Fig. 6(a), while ensuring a smooth transition between the two parts of Equation (8) at 1.6 MeV.

VI. CONCLUSIONS

The response of Fujifilm BAS-TR image plates to laser-driven protons has been absolutely calibrated up to 40 MeV, the range of energies relevant to current research activities using petawatt-class lasers. Proton numbers were determined using CR-39 nuclear track detectors across the entire energy range, using slotted CR-39 placed in front of the IP for low (<10 MeV) energies, and placed behind the IP with various Fe and Cu filters for high energies. The response, which is in broad agreement with previous works, has been described in terms of the existing models and an empirical fitting as a function of the incident proton energy has been deduced. As the BAS-TR brand of IP is a very popular detector employed, for example, in Thomson parabola spectrometers, this calibration will prove useful in determining accurately proton spectra from future high power laser acceleration experiments.

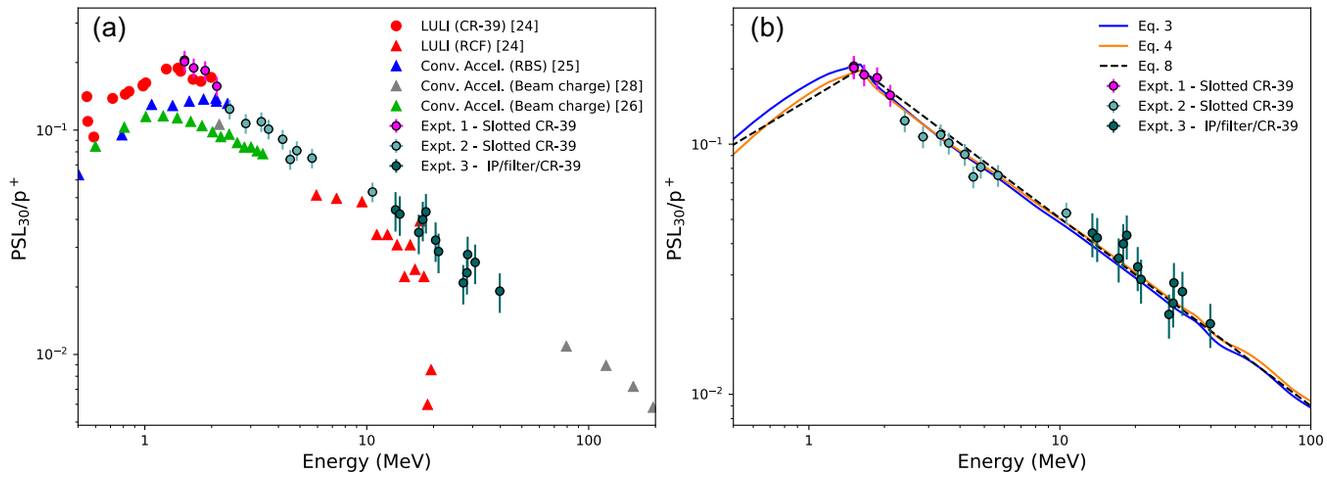

~

A. Macchi, M. Borghesi, and M. Passoni, "Ion acceleration by superintense laser-plasma interaction," Rev. Mod. Phys. **85**, 751–793 (2013), 1302.1775.
B. Dromey, M. Coughlan, L. Senje, M. Taylor, S. Kuschel, B. Villagomez-Bernabe, R. Stefanuik, G. Nersisyan, L. Stella, J. Kohanoff, M. Borghesi, F. Currell, D. Riley, D. Jung, C.-G. Wahlström, C. Lewis, and M. Zepf, "Picosecond metrology of laser-driven proton bursts," Nat. Commun. **7**, 10642 (2016).
M. Borghesi, A. J. Mackinnon, D. H. Campbell, D. G. Hicks, S. Kar, P. K. Patel, D. Price, L. Romagnani, A. Schiavi, and O. Willi, "Multi-mev proton source investigations in ultraintense laser-foil interactions," Phys. Rev. Lett. **92**, 055003 (2004).
T. E. Cowan, J. Fuchs, H. Ruhl, A. Kemp, P. Audebert, M. Roth, R. Stephens, I. Barton, A. Blazevic, E. Brambrink, J. Cobble, J. Fernández, J.-C. Gauthier, M. Geissel, M. Hegelich, J. Kaae, S. Karsch, G. P. Le Sage, S. Letzring, M. Manclossi, S. Meyroneinc, A. Newkirk, H. Pépin, and N. Renard-LeGalloudec, "Ultralow emittance, multi-mev proton beams from a laser virtual-cathode plasma accelerator," Phys. Rev. Lett. **92**, 204801 (2004).
D. Doria, K. F. Kakolee, S. Kar, S. K. Litt, F. Fiorini, H. Ahmed, S. Green, J. C. G. Jeynes, J. Kavanagh, D. Kirby, K. J. Kirkby, C. L. Lewis, M. J. Merchant, G. Nersisyan, R. Prasad, K. M. Prise, G. Schettino, M. Zepf, and M. Borghesi, "Biological effectiveness on live cells of laser driven protons at dose rates exceeding 109 Gy/s," AIP Adv. **2** (2012), 10.1063/1.3699063.
F. Hanton, P. Chaudhary, D. Doria, D. Gwynne, C. Maiorino, C. Scullion, H. Ahmed, T. Marshall, K. Naughton, L. Romagnani, S. Kar, G. Schettino, P. McKenna, S. Botchway, D. R. Symes, P. P. Rajeev, K. M. Prise, and M. Borghesi, "DNA DSB Repair Dynamics following Irradiation with Laser-Driven Protons at Ultra-High Dose Rates," Sci. Rep. **9**, 1–10 (2019).
P. K. Patel, A. J. Mackinnon, M. H. Key, T. E. Cowan, M. E. Foord, M. Allen, D. F. Price, H. Ruhl, P. T. Springer, and R. Stephens, "Isochoric heating of solid-density matter with an ultrafast proton beam," Phys. Rev. Lett. **91**, 125004 (2003).
J. Honrubia, J. Fernández, B. Hegelich, M. Murakami, and C. Enriquez, "Fast ignition driven by quasi-monoenergetic ions: Optimal ion type and reduction of ignition energies with an ion beam array," Laser and Particle Beams **32**, 419–427 (2014).
M. Borghesi, A. Schiavi, D. H. Campbell, M. G. Haines, O. Willi, A. J. MacKinnon, L. A. Gizzi, M. Galimberti, R. J. Clarke, and H. Ruhl, "Proton imaging: a diagnostic for inertial confinement fusion/fast ignitor studies," Plasma Physics and Controlled Fusion **43**, A267–A276 (2001).
L. Romagnani, J. Fuchs, M. Borghesi, P. Antici, P. Audebert, F. Ceccherini, T. Cowan, T. Grismayer, S. Kar, A. Macchi, P. Mora, G. Pretzler, A. Schiavi, T. Toncian, and O. Willi, "Dynamics of electric fields driving the laser acceleration of multi-MeV protons," Phys. Rev. Lett. **95**, 4–7 (2005).
S. C. Wilks, A. B. Langdon, T. E. Cowan, M. Roth, M. Singh, S. Hatchett, M. H. Key, D. Pennington, A. MacKinnon, and R. A. Snavely, "Energetic proton generation in ultra-intense laser-solid interactions," Phys. Plasmas **8**, 542–549 (2001).
F. Wagner, O. Deppert, C. Brabetz, P. Fiala, A. Kleinschmidt, P. Poth, V. A. Schanz, A. Tebartz, B. Zielbauer, M. Roth, T. Stöhlker, and V. Bagnoud, "Maximum Proton Energy above 85 MeV from the Relativistic Interaction of Laser Pulses with Micrometer Thick CH2 Targets," Phys. Rev. Lett. **116**, 1–5 (2016).
T. Esirkepov, M. Borghesi, S. V. Bulanov, G. Mourou, and T. Tajima, "Highly efficient relativistic-ion generation in the laser-piston regime," Phys. Rev. Lett. **92**, 2–5 (2004).
B. Qiao, M. Zepf, M. Borghesi, B. Dromey, M. Geissler, A. Karmakar, and P. Gibbon, "Radiation-pressure acceleration of ion beams from nanofoil targets: The leaky light-sail regime," Phys.

Rev. Lett. **105**, 8–11 (2010).
L. Yin, B. J. Albright, B. M. Hegelich, and J. C. Fernández, "Gev laser ion acceleration from ultrathin targets: The laser break-out afterburner," Laser and Particle Beams **24**, 291–298 (2006).
L. Yin, B. J. Albright, K. J. Bowers, D. Jung, J. C. Fernández, and B. M. Hegelich, "Three-dimensional dynamics of breakout afterburner ion acceleration using high-contrast short-pulse laser and nanoscale targets," Phys. Rev. Lett. **107**, 1–4 (2011).
A. Higginson, R. J. Gray, M. King, N. Butler, R. J. Dance, S. D. R. Willaimson, R. Capdessus, R. Wilson, C. Armstrong, S. J. Hawkes, J. S. Green, P. Martin, W. Q. Wei, X. H. Yuan, S. R. Mirfayzi, S. Kar, R. J. Clarke, D. Neely, and P. McKenna, "Near-100 MeV protons via a laser-driven transparency-enhanced hybrid acceleration scheme," Nat. Commun. **9** (2018), 10.1038/s41467-018-03063-9.
T. Ziegler, D. Albach, C. Bernert, S. Bock, F.-E. Brack, T. E. Cowan, N. P. Dover, M. Garten, L. Gaus, R. Gebhardt, I. Goethel, U. Helbig, A. Irman, H. Kiriyama, T. Kluge, A. Kon, S. Kraft, F. Kroll, M. Loeser, J. Metzkes-Ng, M. Nishiuchi, L. Obst-Huebl, T. Püschel, M. Rehwald, H.-P. Schlenvoigt, U. Schramm, and K. Zeil, "Proton beam quality enhancement by spectral phase control of a PW-class laser system - Scientific Reports," Sci. Rep. **11**, 1–7 (2021).
P. R. Bolton, M. Borghesi, C. Brenner, D. C. Carroll, C. De Martinis, A. Flacco, V. Floquet, J. Fuchs, P. Gallegos, D. Giove, J. S. Green, S. Green, B. Jones, D. Kirby, P. McKenna, D. Neely, F. Nuesslin, R. Prasad, S. Reinhardt, M. Roth, U. Schramm, G. G. Scott, S. Ter-Avetisyan, M. Tolley, G. Turchetti, and J. J. Wilkens, "Instrumentation for diagnostics and control of laser-accelerated proton (ion) beams," Phys. Medica **30**, 255–270 (2014).
S. Kar, M. Borghesi, L. Romagnani, S. Takahashi, A. Zayats, V. Malka, S. Fritzler, and A. Schiavi, "Analysis of latent tracks for MeV protons in CR-39," J. Appl. Phys. **101** (2007), 10.1063/1.2433744.
K. Harres, M. Schollmeier, E. Brambrink, P. Audebert, A. Blažević, K. Flippo, D. C. Gautier, M. Geißel, B. M. Hegelich, F. Nürnberg, J. Schreiber, H. Wahl, and M. Roth, "Development and calibration of a Thomson parabola with microchannel plate for the detection of laser-accelerated MeV ions," Rev. Sci. Instrum. **79**, 093306 (2008).
T. W. Jeong, P. K. Singh, C. Scullion, H. Ahmed, K. F. Kakolee, P. Hadjisolomou, A. Alejo, S. Kar, M. Borghesi, and S. Ter-Avetisyan, "Experimental evaluation of the response of microchannel plate detector to ions with 10s of MeV energies," Rev. Sci. Instrum. **87**, 0–7 (2016).
A. McIlvenny, D. Doria, L. Romagnani, H. Ahmed, P. Martin, S. WIlliamson, E. Ditter, O. Ettlinger, G. Hicks, P. McKenna, Z. Najmudin, D. Neely, S. Kar, and M. Borghesi, "Absolute calibration of microchannel plate detector for carbon ions up to 250 MeV," J. Instrum. **14**, C04002–C04002 (2019).
A. Mančić, J. Fuchs, P. Antici, S. A. Gaillard, and P. Audebert, "Absolute calibration of photostimulable image plate detectors used as (0.5-20 MeV) high-energy proton detectors," Rev. Sci. Instrum. **79**, 0–6 (2008).
T. Bonnet, M. Comet, D. Denis-Petit, F. Gobet, F. Hannachi, M. Tarisien, M. Versteegen, and M. M. Aleonard, "Response functions of Fuji imaging plates to monoenergetic protons in the energy range 0.6-3.2 MeV," Rev. Sci. Instrum. **84**, 0–6 (2013).
C. G. Freeman, G. Fiksel, C. Stoeckl, N. Sinenian, M. J. Canfield, G. B. Graeper, A. T. Lombardo, C. R. Stillman, S. J. Padalino, C. Mileham, T. C. Sangster, and J. A. Frenje, "Calibration of a Thomson parabola ion spectrometer and Fujifilm imaging plate detectors for protons, deuterons, and alpha particles," Rev. Sci. Instrum. **82**, 1–6 (2011).
S. Kojima, T. Miyatake, S. Inoue, T. H. Dinh, N. Hasegawa, M. Mori, H. Sakaki, M. Nishiuchi, N. P. Dover, Y. Yamamoto, T. Sasaki, F. Ito, K. Kondo, T. Yamanaka, M. Hashida, S. Sakabe, M. Nishikino, and K. Kondo, "Absolute response of a Fuji BAS-TR imaging plate to low-energy protons (<0.2 MeV) and carbon ions (<1 MeV)," Rev. Sci. Instrum. **92**, 033306 (2021).
N. Rabhi, D. Batani, G. Boutoux, J. E. Ducret, K. Jakubowska, I. Lantuejoul-Thfoin, C. Nauraye, A. Patriarca, A. Saïd, A. Semsoum, L. Serani, B. Thomas, and B. Vauzour, "Calibration of imaging plate detectors to mono-energetic protons in the range 1-200 MeV," Rev. Sci. Instrum. **88** (2017), 10.1063/1.5009472.
I. J. Paterson, R. J. Clarke, N. C. Woolsey, and G. Gregori, "Image plate response for conditions relevant to laser-plasma interaction experiments," Meas. Sci. Technol. **19**, 095301 (2008).
A. Alejo, S. Kar, H. Ahmed, A. G. Krygier, D. Doria, R. Clarke, J. Fernandez, R. R. Freeman, J. Fuchs, A. Green, J. S. Green, D. Jung, A. Kleinschmidt, C. L. S. Lewis, J. T. Morrison, Z. Najmudin, H. Nakamura, G. Nersisyan, P. Norreys, M. Notley, M. Oliver, M. Roth, J. A. Ruiz, L. Vassura, M. Zepf, and M. Borghesi, "Characterisation of deuterium spectra from laser driven multi-species sources by employing differentially filtered image plate detectors in Thomson spectrometers," Rev. Sci. Instrum. **85**, 0–7 (2014), 1408.2978.
G. Boutoux, N. Rabhi, D. Batani, A. Binet, J. E. Ducret, K. Jakubowska, J. P. Nègre, C. Reverdin, and I. Thfoin, "Study of imaging plate detector sensitivity to 5-18 MeV electrons," Rev. Sci. Instrum. **86** (2015), 10.1063/1.4936141.
D. O. Golovin, S. R. Mirfayzi, S. Shokita, Y. Abe, Z. Lan, Y. Arikawa, A. Morace, T. A. Pikuz, and A. Yogo, "Calibration of imaging plates sensitivity to high energy photons and ions for laser-plasma interaction sources," Journal of Instrumentation **16** (2021), 10.1088/1748-0221/16/02/T02005.
D. Doria, S. Kar, H. Ahmed, A. Alejo, J. Fernandez, M. Cerchez, R. J. Gray, F. Hanton, D. A. MacLellan, P. McKenna, Z. Najmudin, D. Neely, L. Romagnani, J. A. Ruiz, G. Sarri, C. Scullion, M. Streeter, M. Swantusch, O. Willi, M. Zepf, and M. Borghesi, "Calibration of BAS-TR image plate response to high energy (3-300 MeV) carbon ions," Rev. Sci. Instrum. **86** (2015), 10.1063/1.4935582.
J. Strehlow, P. Forestier-Colleoni, C. McGuffey, M. Bailly-Grandvaux, T. S. Daykin, E. McCary, J. Peebles, G. Revet, S. Zhang, T. Ditmire, M. Donovan, G. Dyer, J. Fuchs, E. W. Gaul, D. P. Higginson, G. E. Kemp, M. Martinez, H. S. McLean, M. Spinks, H. Sawada, and F. N. Beg, "The response function of fujifilm bas-tr imaging plates to laser-accelerated titanium ions," Review of Scientific Instruments **90**, 083302 (2019), https://doi.org/10.1063/1.5109783.
T. Bonnet, M. Comet, D. Denis-Petit, F. Gobet, F. Hannachi, M. Tarisien, M. Versteegen, and M. M. Aléonard, "Response functions of imaging plates to photons, electrons and 4He particles," Rev. Sci. Instrum. **84**, 103510 (2013).
http://www.srim.org.
J. F. Ziegler, M. D. Ziegler, and J. P. Biersack, "SRIM - The stopping and range of ions in matter (2010)," Nucl. Instruments Methods Phys. Res. Sect. B Beam Interact. with Mater. Atoms **268**, 1818–1823 (2010).
V. Lelasseux and J. Fuchs, "Modelling energy deposition in TR image plate detectors for various ion types," Journal of Instrumentation **15**, P04002–P04002 (2020).
M. Nishiuchi, H. Sakaki, N. P. Dover, T. Miyahara, K. Shiokawa, S. Manabe, T. Miyatake, K. Kondo, K. Kondo, Y. Iwata, Y. Watanabe, and K. Kondo, "Ion species discrimination method by linear energy transfer measurement in Fujifilm BAS-SR imaging plate," Review of Scientific Instruments **91** (2020), 10.1063/5.0016515.
J. B. Birks, "Scintillations from Organic Crystals: Specific Fluorescence and Relative Response to Different Radiations," Proc. Phys. Soc. A **64**, 874–877 (1951).
T. Dzelzainis, G. Nersisyan, D. Riley, L. Romagnani, H. Ahmed, A. Bigongiari, M. Borghesi, D. Doria, B. Dromey, M. Makita, S. White, S. Kar, D. Marlow, B. Ramakrishna, G. Sarri, M. Zaka-Ul-Islam, M. Zepf, and C. L. S. Lewis, "The TARANIS laser: A multi-Terawatt system for laser-plasma investigations," Laser Part. Beams **28**, 451–461 (2010).

M. Kanasaki, S. Jinno, H. Sakaki, K. Kondo, K. Oda, T. Yamauchi, and Y. Fukuda, "The precise energy spectra measurement of laser-accelerated MeV/n-class high-Z ions and protons using CR-39 detectors," Plasma Phys. Control. Fusion **58** (2016), 10.1088/0741-3335/58/3/034013.

R. Prasad, D. Doria, S. Ter-Avetisyan, P. S. Foster, K. E. Quinn, L. Romagnani, C. M. Brenner, J. S. Green, P. Gallegos, M. J. V. Streeter, D. C. Carroll, O. Tresca, N. Dover, C. A. J. Palmer, J. Schreiber, D. Neely, Z. Najmudin, P. McKenna, M. Zepf, and M. Borghesi, "Calibration of Thomson parabola-MCP assembly for multi-MeV ion spectroscopy," Nucl. Instruments Methods Phys. Res. Sect. A Accel. Spectrometers, Detect. Assoc. Equip. **623**, 712–715 (2010).

D. Doria, P. Martin, H. Ahmed, A. Alejo, M. Cerchez, S. Ferguson, J. Fernandez-Tobias, J. S. Green, D. Gwynne, F. Hanton, J. Jarrett, D. A. Maclellan, A. McIlvenny, P. McKenna, J. A. Ruiz, M. Swantusch, O. Willi, S. Zhai, M. Borghesi, and S. Kar, "Calibration of BAS-TR image plate response to GeV gold ions," Rev. Sci. Instrum. **93**, 033304 (2022).

D. Jung, R. Hörlein, D. Kiefer, S. Letzring, D. C. Gautier, U. Schramm, C. Hübsch, R. Öhm, B. J. Albright, J. C. Fernandez, D. Habs, and B. M. Hegelich, "Development of a high resolution and high dispersion Thomson parabola," Rev. Sci. Instrum. **82** (2011), 10.1063/1.3523428.

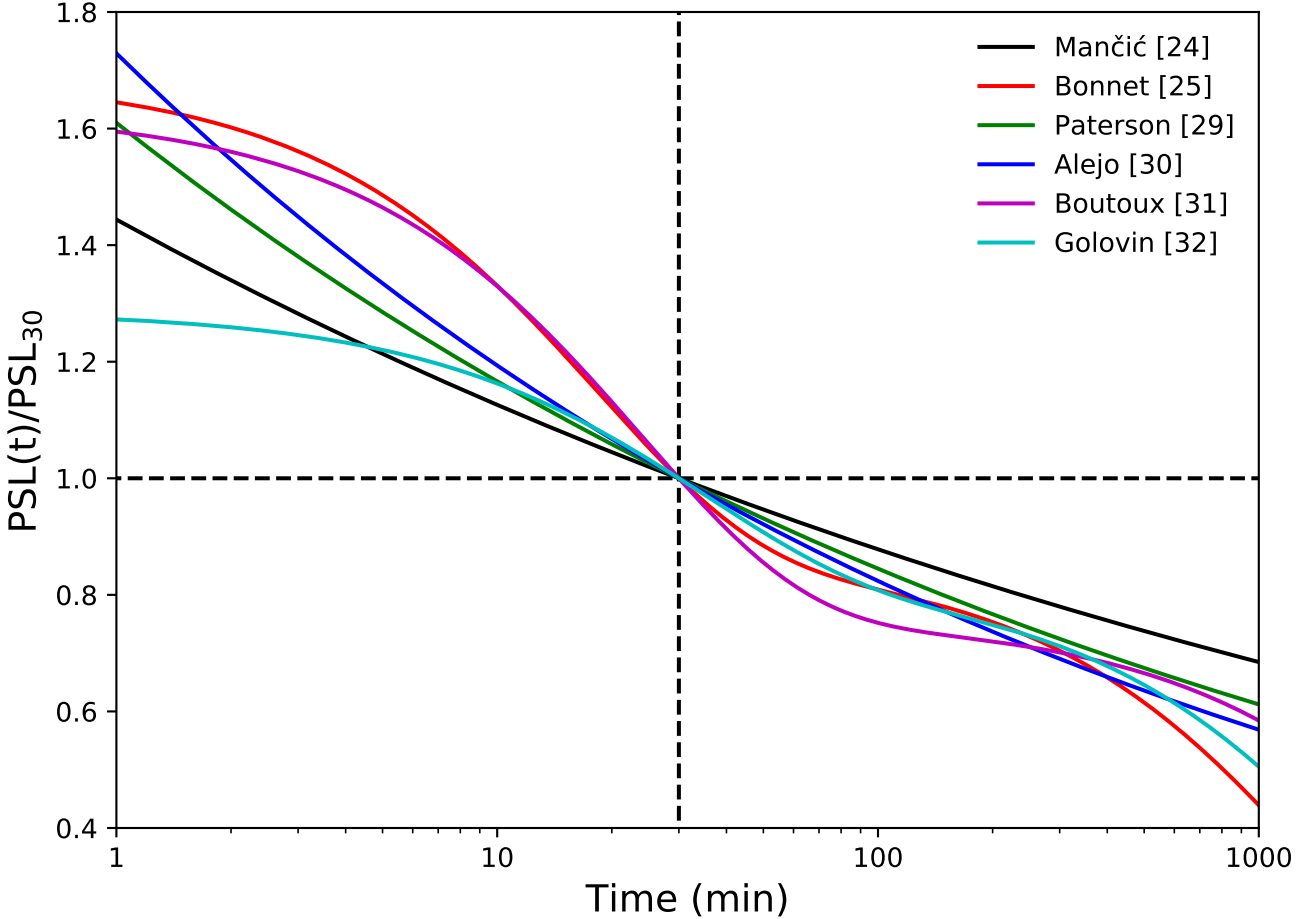
Mančić [24]
Bonnet [25]
Paterson [29]
Alejo [30]
Boutoux [31]
Golovin [32]
PSL(t)/PSL30
Time (min)
1.8
1.6
1.4
1.2
1.0
0.8
0.6
0.4
1
10
100
1000

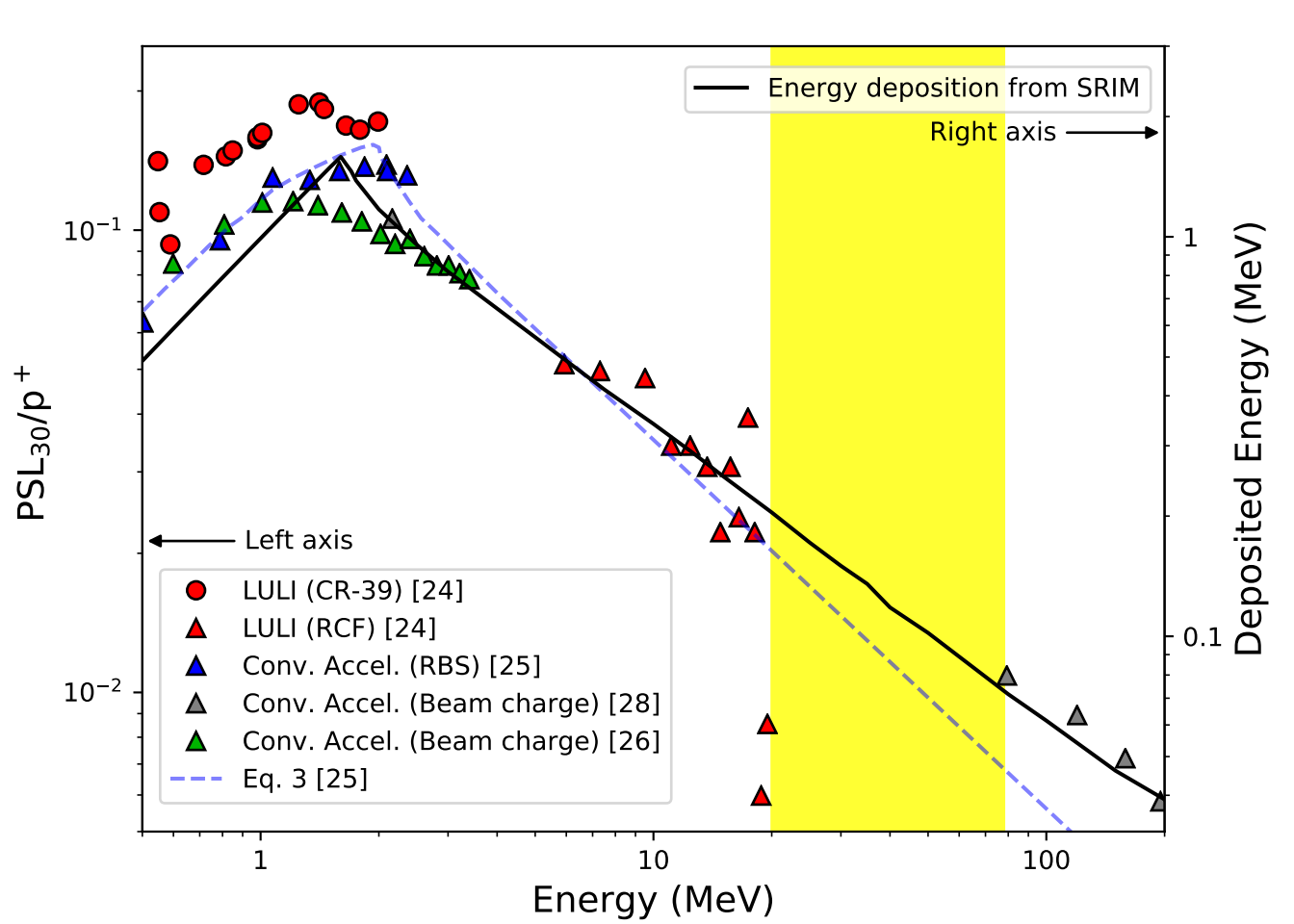
Energy deposition from SRIM
Right axis
Left axis
LULI (CR-39) [24]
LULI (RCF) [24]
Conv. Accel. (RBS) [25]
Conv. Accel. (Beam charge) [28]
Conv. Accel. (Beam charge) [26]
Eq. 3 [25]
PSL_{30}/p^+
Deposited Energy (MeV)
Energy (MeV)
10^{-1}
10^{-2}
1
0.1
1
10
100

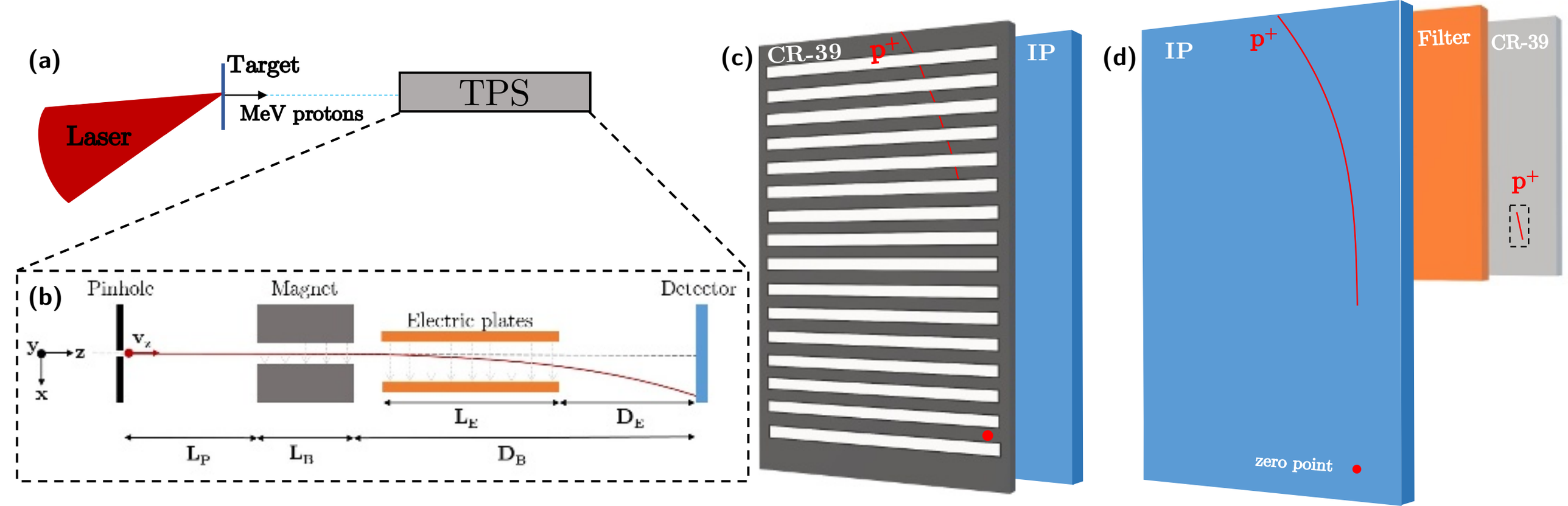
(a)
Target
TPS
MeV protons
Laser
(b)
Pinhole
Magnet
Detector
Electric plates
y
z
x
v_z
L_E
D_E
L_P
L_B
D_B
(c)
CR-39
p^+
IP
(d)
IP
p^+
Filter
CR-39
p^+
zero point

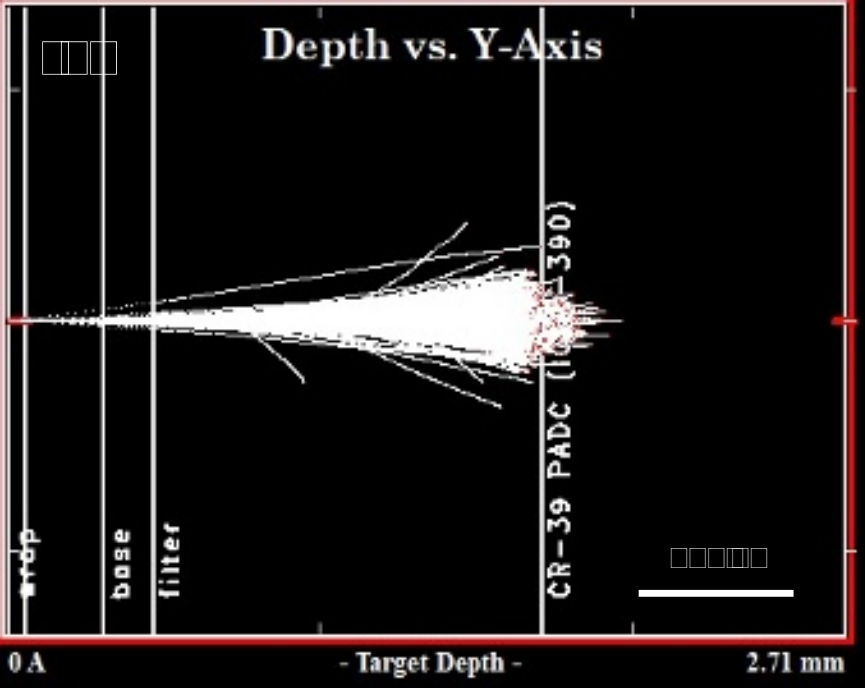
Depth vs. Y-Axis
drop
base
filter
CR-39 PADC
0 A
- Target Depth -
2.71 mm

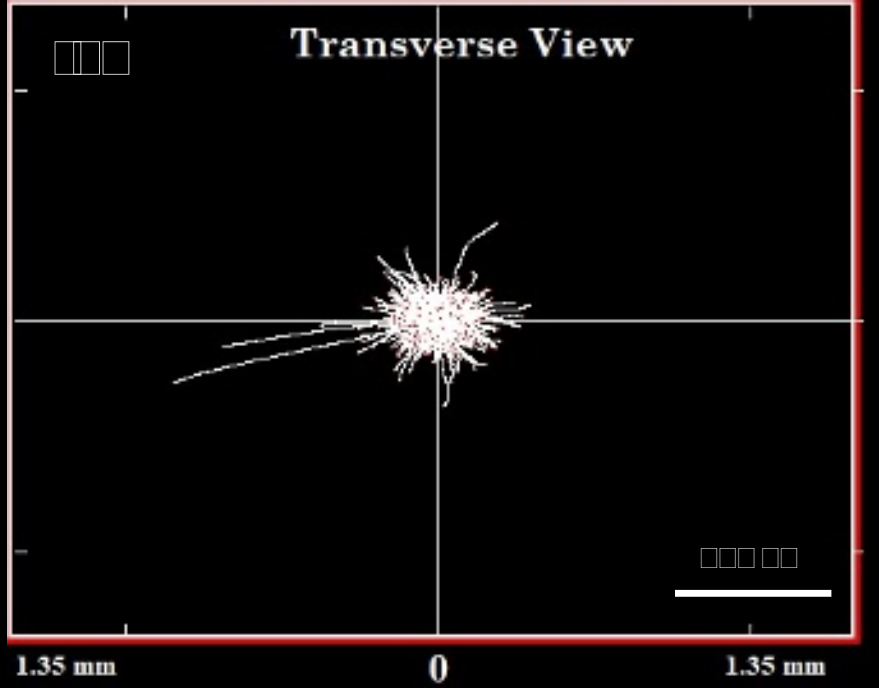
Transverse View
1.35 mm
0
1.35 mm

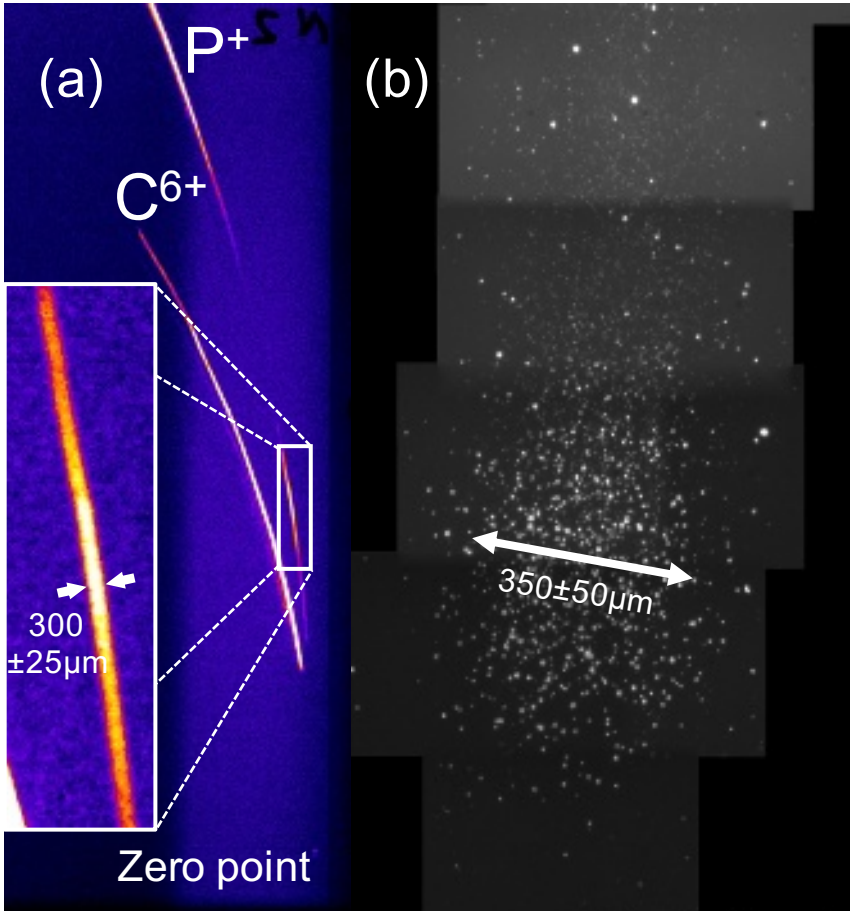
(a)
P+
C6+
300
±25μm
Zero point

(b)
350±50μm

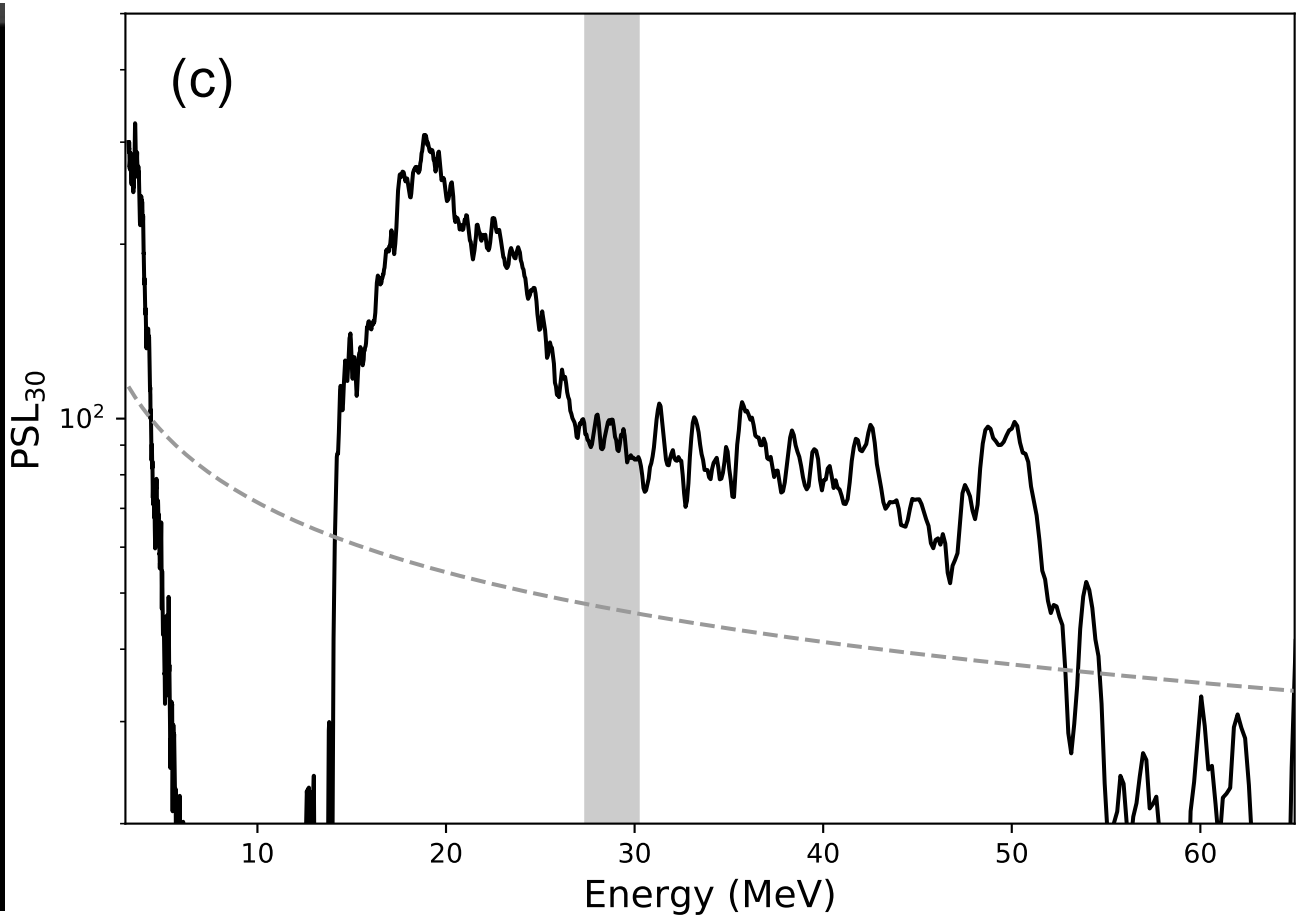
(c)
PSL30
10²
10
20
30
40
50
60
Energy (MeV)

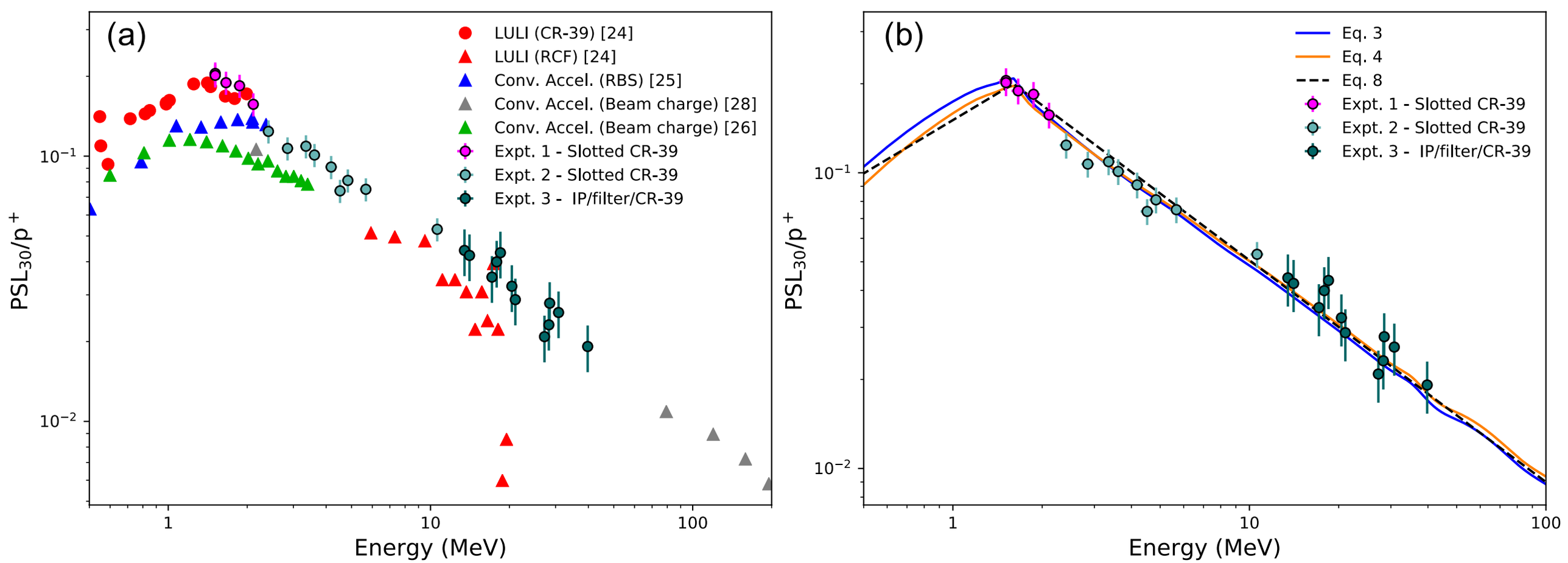
(a)
LULI (CR-39) [24]
LULI (RCF) [24]
Conv. Accel. (RBS) [25]
Conv. Accel. (Beam charge) [28]
Conv. Accel. (Beam charge) [26]
Expt. 1 - Slotted CR-39
Expt. 2 - Slotted CR-39
Expt. 3 - IP/filter/CR-39
PSL30/p+
Energy (MeV)
(b)
Eq. 3
Eq. 4
Eq. 8
Expt. 1 - Slotted CR-39
Expt. 2 - Slotted CR-39
Expt. 3 - IP/filter/CR-39
PSL30/p+
Energy (MeV)